

OPEN ACCESS

On the Thermodynamic Origin of the Formation of Li-Dendrites in an Electrochemical Cell

To cite this article: Yudong Wang et al 2021 J. Electrochem. Soc. 168 100503

View the <u>article online</u> for updates and enhancements.





On the Thermodynamic Origin of the Formation of Li-Dendrites in an Electrochemical Cell

Yudong Wang, 1,2,* 10 Anil V. Virkar, 1,3,** and Xiao-Dong Zhou 1,2,**,z

The direction of growth of neutral species in batteries and electrolyzers differs significantly. In a battery, dendrites can be formed during the charging process and are perpendicular to the interface between electrode and electrolyte. The aim of this manuscript is to address the origin of the growth orientation of the neutral metal and elucidate the factors that govern the dendrite growth by using the concept of chemical potential of neutral lithium and the electronic current in the electrolyte. With the consideration of the electronic conductivity in the ionic conductive phases, the chemical potential difference of lithium could be calculated across the cell, and predicts lithium deposition in the solid-electrolyte interphase (SEI) layer. The electronically conducting metal precipitate could work as a part of electrode and allow further growth along the current direction, resulting in the formation of dendrites. During growth, the ionic conductivity and the thickness distribution of the SEI layer determine the growth kinetics and the dendrite shape. A lower ionic conductivity and a nonuniform SEI layer lead to a sharp lithium dendrite. On the other hand, a low electronic conductivity and a high ionic conductivity of the electrode/electrolyte interface are in favor of suppressing the formation of a neutral species.

© 2021 The Author(s). Published on behalf of The Electrochemical Society by IOP Publishing Limited. This is an open access article distributed under the terms of the Creative Commons Attribution 4.0 License (CC BY, http://creativecommons.org/licenses/by/4.0/), which permits unrestricted reuse of the work in any medium, provided the original work is properly cited. [DOI: 10.1149/1945-7111/ac1971]

Manuscript submitted March 23, 2021; revised manuscript received June 26, 2021. Published October 12, 2021.

Chemical potential of M in the cathode (J mol⁻¹)

Chemical potential of lithium in the anode

 $(J \text{ mol}^{-1})$

¹Institute for Materials Research and Innovation, University of Louisiana at Lafayette, Lafayette, Louisiana 70504, United States of America

²Depariment of Chemical Engineering, University of Louisiana at Lafayette, Lafayette, Louisiana 70504, United States of America

³Department of Materials Science and Engineering, University of Utah, Salt Lake City, Utah 84102, United States of America

^{*}Electrochemical Society Student Member.

^{**}Electrochemical Society Fellow.

^zE-mail: zhou@louisiana.edu

μ_{Li}^c	Chemical potential of lithium in the cathode (J mol ⁻¹)
$ ilde{\mu}_i$	Electrochemical potential of species i (J mol ⁻¹)
σ_i	Ionic conductivity (S m ⁻¹)
$\sigma_{\!\scriptscriptstyle e}$	Electronic conductivity (S m ⁻¹)
$egin{array}{l} \sigma_e \ \sigma_i^{el} \ \sigma_e^{el} \ \sigma_i^{SEI} \ \sigma_e^{SEI} \ \sigma_i^{CEI} \ \sigma_e^{CEI} \ \end{array}$	Ionic conductivity of the electrolyte (S m ⁻¹)
σ_e^{el}	Electronic conductivity of the electrolyte (S m ⁻¹)
σ_i^{SEI}	Ionic conductivity of the SEI (S m ⁻¹)
σ_{ρ}^{SEI}	Electronic conductivity of the SEI (S m ⁻¹)
σ_i^{CEI}	Ionic conductivity of the CEI (S m ⁻¹)
σ_{a}^{CEI}	Electronic conductivity of the CEI (S m ⁻¹)
Φ	Electrostatic potential (V)
$\varphi = -\frac{\mu_{e^{-}}}{F} + \Phi$	Electrical potential (V)
φ^a F	The electrical potential of anode (V)
φ^c	The electrical potential of cathode (V)
ϕ	Fugacity coefficient of a gas
$\dot{\Omega}$	The lithium precipitate

The precipitation of neutral species is ubiquitous in an electrolytic cell (i.e. a charging mode) to form Li-metal, O_2 , and H_2 , which remains a critical issue in rechargeable batteries and electrolyzers. For instance, cracks (Fig. 1a) were observed in solid oxide electrolysis cells due to the precipitation of oxygen. These cracks increase the resistance of an electrolyzer, decrease its efficiency, and even lead to a complete delamination of the electrode from the solid electrolyte. 1,2

The surface of lithium precipitate

 $\partial\Omega$

Another example is the deposition of metal-dendrites (Fig. 1b) for species such as Li, Na, and Zn. Metal dendrites are formed near the negative electrode of a battery during the charging process. The sharp metal dendrite can punch through the separator, leading to a short circuit of the battery. As a result, the formation of dendrites becomes a serious safety issue in the batteries with a metal-based electrode. 5-7 A distinctive difference among these precipitates, oxygen vs lithium, is that the relative orientation of cracks/dendrites is different in the two cases in relation to electrolyte/electrode interfaces and the direction of current. The origin for such a distinctive difference has remained elusive.

It is known that the transport properties of the neutral species ^{8,9} play a key role in the evolution of a neutral species due to the change of the potential profile in the electrolyte. The evolution of a neutral species involves migration of multiple species in a series of chemical and electrochemical reaction processes. These processes are almost always coupled. Simplifications, however, are often made, such as, for example, assuming that transport of a species occurs only down its own chemical potential gradient. Such simplifications mean that the coupling terms are entirely ignored and that the all-important effects associated with linear non-equilibrium and nonlinear

non-equilibrium thermodynamics are left untreated. These oversimplifications ignore the fundamentals of irreversible thermodynamics and the resulting kinetics associated with coupling. Thus, it renders the analysis incapable of producing reliable predications.

Proper treatment of the problem requires formulating the governing equations within the context of non-equilibrium thermodynamics. For systems close to equilibrium, Onsager equations allow one to explore coupling between fluxes of various species, and forms the subject of linear non-equilibrium thermodynamics. Onsager equations are given by $J_i = \sum_{i} L_{ik} X_k$, where X_k is the

Onsager equations are given by $J_i = \sum_k L_{ik} X_k$, where X_k is the thermodynamic force on k, J_i is the thermodynamic flux of i, and L_{ik} are the Onsager coefficients. ¹⁰ Thermodynamic coupling is described by nonzero cross terms, that is by $L_{ik} \neq 0$.

The basic tenets of non-equilibrium thermodynamics under the assumption of *local equilibrium* (assumption that is valid even in systems far removed from equilibrium) lead to the conclusion that even in electrolyte membranes, the electronic conductivity cannot be set to zero *mathematically*. That is, the description of transport requires that electronic conduction through predominantly ionic conductors be taken into account, no matter how small the electronic conductivity is. This immediately calls into question a commonly made assumption of zero electronic current through an electrolyte, which prevents the evaluation of the chemical potential of electrically neutral species corresponding to the mobile ion.

For example, μ_{Li} —which is the chemical potential of neutral lithium in a lithium ion (Li⁺) conductor, such as the electrolyte of a Li-ion battery—cannot be determined if one assumes that the electronic conductivity of the electrolyte is mathematically zero. The low-level electronic conduction is in part the source of the Onsager cross terms and thus cannot be neglected, even when the predominant current through an electrolyte is ionic. By considering the electronic conductivity, the chemical potential of neutral species in the electrolyte can be calculated based on the local chemical equilibrium. The local equilibrium assumption provides full coupling between the driving forces and leads to reduced but a complete set of variables to simulate the operation of an electrochemical system. $^{9,11-13}$

In this work, linear non-equilibrium thermodynamics and the assumption of local chemical and thermodynamic equilibrium are applied to investigate the formation and evolution of lithium precipitates near lithium metal anode. The formation and the evolution of an electrically conductive lithium dendrite is simulated in the lithium electrochemical deposition system based on the calculation of the measurable potentials. The growth rate and the geometry of the lithium dendrite are highly dependent on the properties of the solid-electrolyte interphase (SEI) layer on the lithium anode.

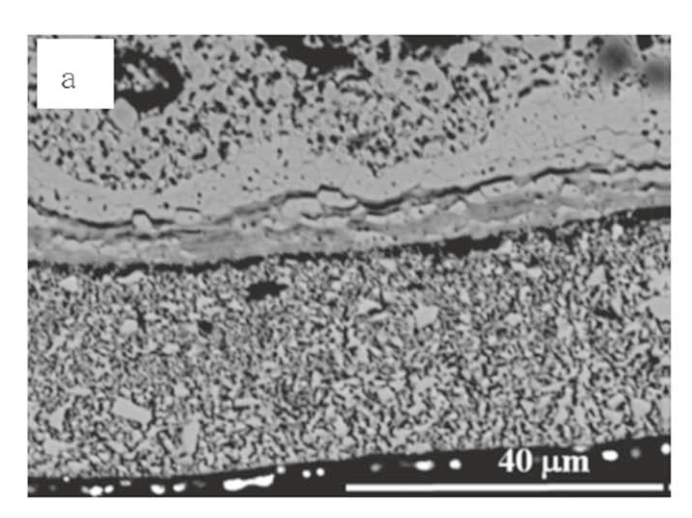




Figure 1. (a) Cracks inside the electrolyte and electrode delamination.³ (b) Lithium metal dendrites in a lithium cell with polymer electrolyte.⁴

Thermodynamic Analysis of Transport in an Electrolyte

In an electrolyte, both ions and electrons/holes are the charge carriers which move in the presence of a thermodynamic potential gradient. The fluxes are considered linear functions of the chemical potential gradients of the species. We assume that constituent mobile ions M^{m+} of valence m^+ , electrons (e $^-$), and the corresponding neutral species (M) are under local thermodynamic and chemical equilibrium in the electrolyte.

$$M(\vec{r}) \rightleftharpoons M^{m+}(\vec{r}) + me^{-}(\vec{r})$$
 [1]

The chemical potentials (μ) of the reactant and products follow Eq. 2 at the position $\vec{r}(x, y, z)$ are given by

$$\mu_M(\vec{r}) = \mu_{M^{m+}}(\vec{r}) + m\mu_{e^-}(\vec{r})$$
 [2]

In what follows the \vec{r} is dropped. The chemical potential can be evaluated by measuring the partial pressure (p_M) and the fugacity coefficient (ϕ_M) in a gas mixture or the concentration (c_M) and the activity coefficient (γ_M) in a solution

$$\mu_M = \mu_M^0 + RT \ln \left(\phi_M \frac{p_M}{p_M^0} \right)$$
 [3]

or

$$\mu_M = \mu_M^0 + RT \ln \left(\gamma_M \frac{c_M}{c_M^0} \right)$$
 [4]

where μ_M^0 is the chemical potential of M at the standard state; c_M^0 and p_M^0 are the concentration and partial pressure of M, respectively, at the defined standard state; R is the gas constant; and T is the absolute temperature.

For charge carriers in an electrolyte, their diffusion can be driven by the electric field and the chemical potential gradient. As a result, the physical property, the electrochemical potential $(\tilde{\mu})$, is needed. The electrochemical potentials of M^{m+} $(\tilde{\mu}_{M^{m+}})$ and electrons $(\tilde{\mu}_{e^{-}})$ are defined as:

$$\tilde{\mu}_{M^{m+}} = \mu_{M^{m+}} + mF\Phi \tag{5}$$

and

$$\tilde{\mu}_{e^-} = \mu_{e^-} - F\Phi \tag{6}$$

where Φ is the electrostatic potential and F is the Faraday constant. The fluxes of ions (J_{M}^{m+}) and electrons $(J_{e^{-}})$, driven by the electrochemical potential gradients, can be written as:

$$J_{M^{m+}} = -\frac{D_{M^{m+}C_{M}^{m+}}}{RT} \nabla \tilde{\mu}_{M^{m+}}$$
 [7]

$$J_{e^{-}} = -\frac{D_{e^{-}}c_{e^{-}}}{RT}\nabla\tilde{\mu}_{e^{-}}$$
 [8]

Applying Eqs. 5 and 6 to Eq. 2, the relation between the chemical potential of neutral species (μ_M) and the electrochemical potentials of M^{m+} $(\tilde{\mu}_M{}^{m+})$ and electrons $(\tilde{\mu}_e{}^-)$ is given by:

$$\mu_M = \tilde{\mu}_{M^{m+}} + m\tilde{\mu}_{e^-} \tag{9}$$

From Eq. 9, one can see that, if the local chemical and thermodynamic equilibrium is established in a finite volume, solving two out of the three potentials $(\mu_M, \tilde{\mu}_M^{m+}, \text{ and } \tilde{\mu}_{e^-})$ will provide all the information on fluxes of the system. The flux of a neutral species (J_M) is coupled to that of ions $(J_{M^{m+}})$ and electrons (J_{e^-}) . Attention,

however, must be paid to the fact that only the chemical potential is measurable based on Eqs. 3 or 4, while Φ cannot be evaluated directly. The cell voltage measured between the two electrodes in an electrochemical device is related to the difference in electrochemical potentials of electrons between the cathode $(\tilde{\mu}_e^c)$ and the anode $(\tilde{\mu}_e^c)$:

Cell Voltage =
$$-\frac{\tilde{\mu}_{e^{-}}^{c}}{F} + \frac{\tilde{\mu}_{e^{-}}^{a}}{F}$$
 [10]

The cell voltage shown in Eq. 10 is the difference between electrical potentials of the cathode and the anode:

Cell Voltage =
$$\varphi^c - \varphi^a$$
 [11]

The electric potential, φ , is defined as:

$$\varphi = -\frac{\tilde{\mu}_{e^-}}{F} = -\frac{\mu_e}{F} + \Phi \tag{12}$$

Thus, φ and μ_M are the two measurable parameters and will be used as the key physical variables in our model. In addition, the diffusion coefficients of the ions and electrons $(D_{M}^{m+}$ and $D_{e^-})$ can be replaced by the measurable conductivities of the ions (σ_i) and electrons (σ_e) in the electrolyte from the Nernst-Einstein relations shown in Eqs. 13 and 14:

$$D_{M^{m+}} = \frac{\sigma_i RT}{c_{M^m} + m^2 F^2}$$
 [13]

and

$$D_{e^{-}} = \frac{\sigma_e RT}{\sigma_e F^2}$$
 [14]

Thus, Eqs. 7 and 8 become:

$$J_{M^{m+}} = -\frac{\sigma_i}{m^2 F^2} \nabla \tilde{\mu}_{M^{m+}}$$
 [15]

$$\boldsymbol{J_{e^{-}}} = -\frac{\sigma_{e}}{E^{2}} \nabla \tilde{\mu}_{e^{-}}$$
 [16]

Equation 12 gives

$$\tilde{\mu}_{e^{-}} = -F\varphi \tag{17}$$

Replacing the electrochemical potential in Eqs. 16 with 17 gives

$$J_{e^{-}} = \frac{\sigma_{e}}{F} \nabla \varphi \tag{18}$$

Equations 9 and 17 give

$$\tilde{\mu}_{M^{m+}} = \mu_M + mF\varphi \tag{19}$$

Replacing $\tilde{\mu}_{M^{m+}}$ in Eqs. 16 with 19 gives:

$$\boldsymbol{J}_{\boldsymbol{M}^{m+}} = -\frac{\sigma_i}{m^2 F^2} \nabla \mu_{\boldsymbol{M}} - \frac{\sigma_i}{mF} \nabla \varphi$$
 [20]

Balance Equations and Boundary Conditions of an Electrochemical Cell

Since both mass and charge are conserved, the divergences of the mass flux and the charge flux are equal to 0 in steady state. The cases considered here are strictly quasi-steady state as will be discussed later. It must be noted that both M^{m+} ions and electrons are transported through the electrolyte, which contribute to I_i and I_e , respectively. In the M^{m+} conductive phases, the balance equations for mass and charge become:

(a) Mass balance.

$$\nabla \cdot (\boldsymbol{J_M} + \boldsymbol{J_M}^{m+}) = 0 \tag{21}$$

(b) Charge balance.

$$\nabla \cdot \mathbf{I}_t = \nabla \cdot (\mathbf{I}_i + \mathbf{I}_e) = 0$$
 [22]

The concentration of neutral species is usually negligible in the electrolyte, due to the large equilibrium constant of reaction (1), indicating $c_M \approx 0.9$ Therefore, the flux of neutral M (J_M) can hardly occur in the electrolyte.

$$J_M \approx 0$$
 [23]

Assuming the ionic conductivity is constant in Eq. 15, Eq. 21 gives

$$\nabla^2 \tilde{\mu}_{M^{m+}} = 0 \tag{24}$$

In Eq. 22 the total current, I_t , is the sum of the ionic (I_i) and the electronic currents (I_e). The current densities are proportional to the fluxes of ions and electrons, respectively.

$$I_{i} = mFJ_{M^{m+}} = -\frac{\sigma_{i}}{mF} \nabla \tilde{\mu}_{M^{m+}}$$
 [25]

$$I_e = -FJ_{e^-} = -\sigma_e \nabla \varphi \tag{26}$$

By assuming constant ionic and electronic conductivities in the electrolyte, Eq. 22 gives

$$-\frac{\sigma_i}{mF} \nabla^2 \tilde{\mu}_{M^{m+}} - \sigma_e \nabla^2 \varphi = 0$$
 [27]

Thus, from Eqs. 19, 24 and 27, the distribution of the electrical potential and the chemical potential of M follows the Laplace equation, assuming the electronic conductivity of electrolyte is constant.

$$\nabla^2 \varphi = 0 \tag{28}$$

$$\nabla^2 \mu_M = 0 \tag{29}$$

The ionic current density can be calculated from the potential gradients after solving Eqs. 28 and 29. The mathematical relation can be derived from Eqs. 19 and 25.

$$I_{i} = -\frac{\sigma_{i}}{mF} \nabla \mu_{M} - \sigma_{i} \nabla \varphi \tag{30}$$

The total current density is the sum of the electronic and the ionic current densities.

$$I_t = I_i + I_e = -\frac{\sigma_i}{mF} \nabla \mu_M - (\sigma_i + \sigma_e) \nabla \varphi$$
 [31]

Owing to the interaction between the electrode and electrolyte, an additional phase which usually has different transport properties forms at the boundary. Typically, at the anode/electrolyte interface, a solid electrolyte interphase (SEI) forms in lithium-ion batteries, which exhibits a lower Li⁺ conductivity^{9,14,15} than the electrolyte. While at the cathode/electrolyte interface, a cathode electrolyte interphase (CEI) layer contributes to the cathode resistance. The Eqs. 21 to 31 are still valid inside these two layers. The resistances between electrolyte and electrodes are mostly contributed by these two layers and the interfacial resistances are ignored compared to the contribution of the whole interphase layer. In other words, the potentials are assumed to be continuous without abrupt changes at the boundaries. Thus, the continuity gives the following boundary conditions listed in Table I between different phases. $n_{SEI,el}$ is the unit normal vector to the electrolyte/SEI interface and $n_{CEI,el}$ is the unit normal vector to the electrolyte/CEI interface.

Table I. Boundary conditions between electrode and electrolyte.

Boundary	Equation	Eq#
Electrolyte/SEI	$arphi^{SEI} = arphi^{el}$	[32]
$(z = z_0)$, ,	
	$\mu_M^{SEI} = \mu_M^{el}$	[33]
	$J_{M^{m+}}^{SEI}{}_{\cdot}n_{SEI,el}=J_{M^{m+}}^{el}{}_{\cdot}n_{SEI,el}$	[34]
	$I_t^{SEI} \cdot n_{SEI,el} = I_t^{el} \cdot n_{SEI,el}$	[35]
Electrolyte/CEI	$arphi^{CEI}=arphi^{el}$	[36]
$(z=z_f)$, ,	
,	$\mu_M^{CEI} = \mu_M^{el}$	[37]
	$J_{M^{m+}}^{CEI} \cdot n_{CEI,el} = J_{M^{m+}}^{el} \cdot n_{CEI,el}$	[38]
	$I_t^{CEI} \cdot n_{CEI,el} = I_t^{el} \cdot n_{CEI,el}$	[39]
SEI/Anode	$\varphi^{SEI} = \varphi^a$	[40]
$(z = z_a)$		
	$\mu_{\scriptscriptstyle M}^{\scriptscriptstyle SEI}=\mu_{\scriptscriptstyle M}^{a}$	[41]
CEI/Cathode	$ \varphi^{CEI} = \varphi^c $	[42]
$(z=z_c)$		
	$\mu_M^{CEI} = \mu_M^{c}$	[43]

With the above partial differential equations (Eqs. 28 and 29) and the boundary conditions, the chemical potential of M (μ_M) and the electrical potential (φ)—two measurable variables—can be solved, which provides a full set of information about the system. Though the equations are derived from the transport of positive ions, they can be used to solve the negative ion transport problems by replacing the valence, m, with the negative valence number. These equations are solved numerically to simulate three-dimensional lithium dendrite evolution. The schematics and plots in this work are performed at the cross-section of a cell in x-z plane.

Electrochemical Lithium Deposition Near a Lithium Metal Anode

The lithium electrodeposition process, which consists of a cylinder-shaped lithium ion electrolyte with a thickness of 40 μ m and two lithium metal electrodes, is simulated with COMSOL Multiphysics and also analytically. Figure 2 shows a schematic. 0.05 V voltage is applied between the two lithium metal electrodes and the chemical potential of metal Li is set as 0 J mol⁻¹ as the reference. The chemical potential in the Li metal electrodes is uniform. The surficial energy change during the electro-deposition both contribute to the interfacial deformation which affects the deposition rate. ¹⁶ In this work, the condition for the dendrite formation and its orientation are addressed. The optimized modelling for the growth rate will be studied in future work.

$$\mu_{Li}(z_a) = \mu_{Li}^a = 0 \text{ J mol}^{-1}$$
 [44]

$$\mu_{Li}(z_c) = \mu_{Li}^c = 0 \text{ J mol}^{-1}$$
 [45]

The variables and their magnitudes for our calculations are listed in Table II. Since the phenomena near the anode are closely investigated in this paper, the cathode, though it is also lithium metal, is assumed to be coated with an artificial CEI with constant σ_i^{CEI} and σ_a^{CEI} in the simulation.

The impact on the lithium deposition of σ_i^{SEI} and σ_e^{SEI} values is studied in the calculation. The SEI layer is widely investigated, and researchers have made tremendous efforts to achieve stable and conductive artificial SEI layers to enhance the cycle life of batteries. Table III provides some examples of SEI layers and their ionic conductivities, which vary from 10^{-6} to $0.1~{\rm S}~{\rm m}^{-1}$. Different

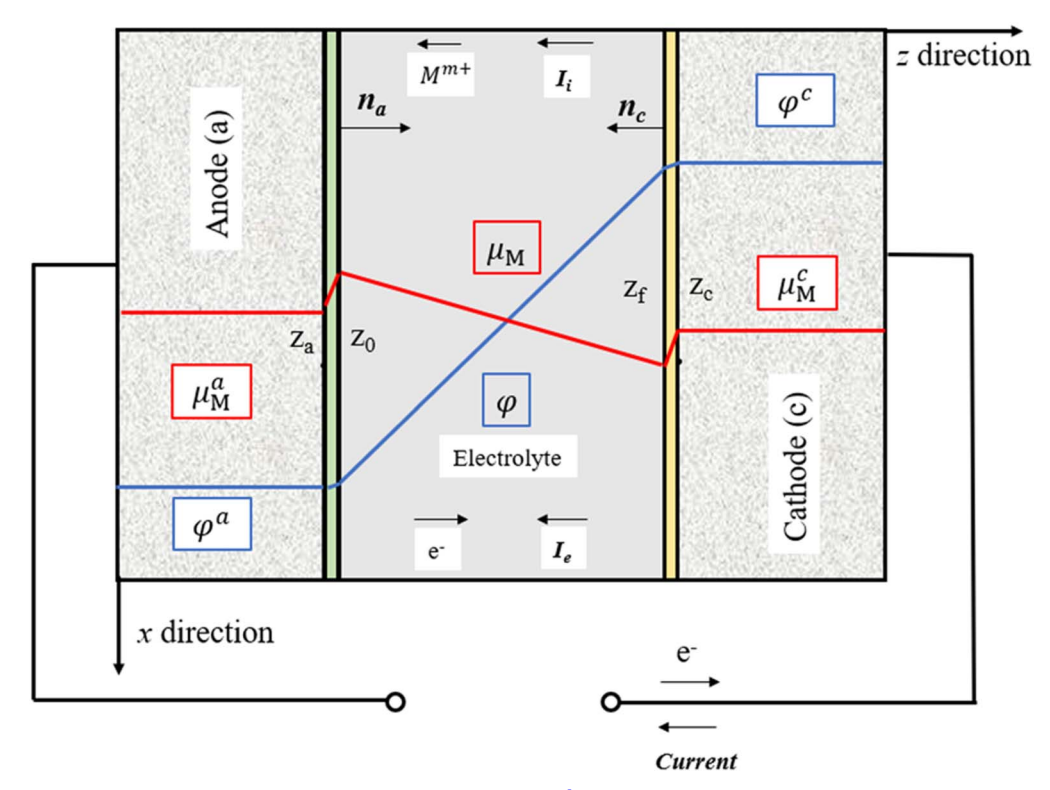


Figure 2. A two-dimensional schematic of a metal plating process at steady state.

Table II. Magnitudes of the variables used in modeling the lithium electrodeposition system. The values listed with a range are the factors studied in the simulation.

Variable	Magnitude	Description
σ_i^{el}	1 [S m ⁻¹] ¹⁷	Ionic conductivity of Li ⁺ in the electrolyte
σ_e^{el}	$10^{-6} [S m^{-1}]$	Electronic conductivity of e in the electrolyte
σ_i^{CEI}	$10^{-1} [S m^{-1}]$	Ionic conductivity of the CEI layer
σ_{e}^{CEI}	$10^{-6} [S m^{-1}]$	Electronic conductivity of the CEI layer
μ_{Li}^a	$0 [J mol^{-1}]$	Lithium chemical potential in the anode
μ_{Li}^c	$0 [J \text{ mol}^{-1}]^{18}$	Lithium chemical potential in the cathode
l	$4 \times 10^{-5} \text{ [m]}$	Thickness of the electrolyte
δ_a	$2 \times 10^{-8} [m]$	Thickness of the SEI layer
δ_c	$2 \times 10^{-8} [m]$	Thickness of the CEI layer
σ_{i}^{SEI}	$10^{-5} \sim 10 \text{ [S m}^{-1]}$	Ionic conductivity of the SEI layer
σ_e^{SEI}	$10^{-10} \sim 1 \text{ [S m}^{-1]}$	Electronic conductivity of the SEI layer
$arphi^a$	0 [V]	Electric potential of the anode
$arphi^c$	0.05 [V]	Electric potential of the cathode

Table III. Chemical composition of various SEI layers and their conductivity in lithium-ion battery application.

Chemical composition	nical composition Ionic conductivity	
Routine SEI	4.2×10 ⁻⁶ S m ⁻¹ @25 °C	20
Li ₃ N	$0.12~{\rm S~m^{-1}~@25~^{\circ}C}$	21, 22
Li ₂ TiO ₃	$2.5 \times 10^{-5} \text{ S m}^{-1} \text{ @}25 \text{ °C}$	23, 24
Polydimethylsiloxane (PDMS)	$\sim 1.6 \times 10^{-3} \text{ S m}^{-1} \text{ @}25 \text{ °C}$	25, 26
LiF	$6 \times 10^{-4} \text{ S m}^{-1} @50 ^{\circ}\text{C}$	27
Li Alginate	1.79×10 ⁻² S m ⁻¹ @25 °C	28
PETMP/ LiBAMB	$3.32 \times 10^{-3} \text{ S m}^{-1} \text{ @}25 \text{ °C}$	29
LLZNO/PEO	$2.2 \times 10^{-3} \text{ S m}^{-1} \text{ @}25 \text{ °C}$	30

artificial SEI layers are designed based on polymer matrix to achieve high lithium conductivity and good mechanical strength. ¹⁹

From Eqs. 26 and 30, one can see that:

$$\nabla \mu_M = -mF \left(\frac{I_i}{\sigma_i} - \frac{I_e}{\sigma_e} \right)$$
 [46]

To obtain the chemical potential difference of M between two different positions (e.g. $r_1(x_1, y_1, z_1)$ and $r_2(x_2, y_2, z_2)$) in the electrolyte, one needs to integrate $\nabla \mu_M \cdot d\mathbf{r}$, which is equal to $\mathbf{d}\mu_M$ —an exact differential and a state function.

$$\mu_{M}(r_{2}) - \mu_{M}(r_{1}) = \int_{r_{1}}^{r_{2}} \nabla \mu_{M} \cdot dr$$
 [47]

Because μ_M is a state function, the integration value is independent of the trajectory selected between r_1 and r_2 during integration at the steady state. With Eq. 47, the integration is given by

$$\mu_{M}(\mathbf{r}_{2}) - \mu_{M}(\mathbf{r}_{1}) = \int_{\mathbf{r}_{1}}^{\mathbf{r}_{2}} -mF\left(\frac{\mathbf{I}_{i} \cdot d\mathbf{r}}{\sigma_{i}} - \frac{\mathbf{I}_{e} \cdot d\mathbf{r}}{\sigma_{e}}\right)$$
[48]

In one dimension (z direction—also the direction for dendrite growth) and assuming steady state and constant conductivities, I_i and I_e should be constant along the z direction from Eqs. 21 and 22. Equation 48 can be simplified as

$$\mu_M(z_2) - \mu_M(z_1) = -mF \left[\frac{I_i(z_2 - z_1)}{\sigma_i} - \frac{I_e(z_2 - z_1)}{\sigma_e} \right]$$
 [49]

As shown in the schematic in Fig. 2, z_a and z_0 are two points on different sides of the SEI layer (shown in blue). Equation 49 becomes

$$\mu_{M}(z_{0}) - \mu_{M}(z_{a}) = -mF \left[I_{i} \frac{(z_{0} - z_{a})}{\sigma_{i}^{SEI}} - I_{e} \frac{(z_{0} - z_{a})}{\sigma_{e}^{SEI}} \right]$$
 [50]

 σ_i^{SEI} and σ_e^{SEI} are the ionic and the electronic conductivities of the SEI layer with a thickness of $\delta_a=z_0-z_a$, respectively.

By replacing M with lithium, Eq. 50 can be written as,

$$\mu_{Li}(z_0) - \mu_{Li}^a = -F \left[I_i \frac{(z_0 - z_a)}{\sigma_i^{SEI}} - I_e \frac{(z_0 - z_a)}{\sigma_e^{SEI}} \right]$$
 [51]

From Eq. 51, one can see that μ_{Li} in the anode SEI layer is not necessarily lower than μ_{Li}^a . The value is dependent on σ_i^{SEI} , σ_e^{SEI} , I_i , and I_e . μ_{Li} and φ in the electrolyte and SEI layer are calculated for various conductivity values of the SEI layer in Fig. 3. As we define μ_{Li}^a is 0, lithium tends to precipitate thermodynamically from the electrolyte when $\mu_{Li} > 0$. An electronically conductive SEI layer with a low σ_i^{SEI} tends to have a high μ_{Li} , which leads to lithium precipitation. The integration of Eqs. 25 and 26 from z_a to z_c gives

$$(\mu_{Li}^c + F\varphi^c) - (\mu_{Li}^a + F\varphi^a) = -FI_i \left(\frac{\delta_c}{\sigma_i^{CEI}} + \frac{\delta_a}{\sigma_i^{SEI}} + \frac{l}{\sigma_i^{el}} \right)$$
[52]

$$\varphi^{c} - \varphi^{a} = -I_{e} \left(\frac{\delta_{c}}{\sigma_{e}^{CEI}} + \frac{\delta_{a}}{\sigma_{e}^{SEI}} + \frac{l}{\sigma_{e}^{el}} \right)$$
 [53]

Then the current densities can be calculated with the measurable values below:

$$I_{i} = -\frac{\frac{\mu_{Li}^{c} - \mu_{Li}^{a}}{F} + \varphi^{c} - \varphi^{a}}{R_{i,t}}$$
 [54]

$$I_e = -\frac{\varphi^c - \varphi^a}{R_{e,t}} \tag{55}$$

Where $R_{i,t}$ is the total ionic ASR of the cell,

$$R_{i,t} = r_i^c + r_i^a + r_i^{el}$$
[56]

$$r_i^c = \frac{\delta_c}{\sigma_c^{CEI}}$$
 [57]

$$r_i^a = \frac{\delta_a}{\sigma_i^{SEI}}$$
 [58]

$$r_i^{el} = \frac{l}{\sigma_i^{el}} \tag{59}$$

And $R_{e,t}$ is the total electronic ASR of the cell,

$$R_{e,t} = \frac{\delta_c}{\sigma_e^{CEI}} + \frac{\delta_a}{\sigma_e^{SEI}} + \frac{l}{\sigma_e^{el}}$$
 [60]

$$r_e^c = \frac{\delta_c}{\sigma_e^{CEI}} \tag{61}$$

$$r_e^a = \frac{\delta_a}{\sigma^{SEI}} \tag{62}$$

$$r_e^{el} = \frac{l}{\sigma_e^{el}} \tag{63}$$

Note that I_i and I_e are negative because the currents in the electrolyte are moving in the -z direction. Then Eq. 51 can be rewritten as

$$\mu_{Li}(z_0) - \mu_{Li}^a = \frac{(\mu_{Li}^c - \mu_{Li}^a) + F(\varphi^c - \varphi^a)}{1 + \frac{r_i^c}{r_i^a} + \frac{r_i^{el}}{r_i^a}} - \frac{(\varphi^c - \varphi^a)F}{1 + \frac{r_e^c}{r_e^a} + \frac{r_e^{el}}{r_e^a}}$$
[64]

For the simulation of the lithium plating process, Eq. 64 can be further simplified with Eqs. 44 and 45

$$\mu_{Li}(z_0) = F(\varphi^c - \varphi^a) \left(\frac{r_i^a}{R_{i,t}} - \frac{r_e^a}{R_{e,t}} \right)$$
 [65]

 $\varphi^c > \varphi^a$ when lithium deposits on the lithium metal anode. Equation 65 shows that a high r_i^a or a low r_e^a will lead to a high μ_{Li} value in the SEI layer. Figure 3 gives the potential distribution with different σ_e^{SEI} and σ_i^{SEI} . The high slope of φ stems from a relatively low σ_e in the region while a low σ_i results in a high slope of $\frac{\tilde{\mu}_{Li}+}{F}$. Figure 3 also predicts lithium precipitation in the SEI layer from the thermodynamic perspective with a high σ_e^{SEI} and low σ_i^{SEI}

from the thermodynamic perspective with a high σ_e^{SLI} and low σ_i^{SLI} in (b), (c) and (f). Therefore, the SEI layer should be a good electronic insulator to prevent lithium precipitation at SEI/electrolyte boundaries. Besides, lithium precipitation requires the participation

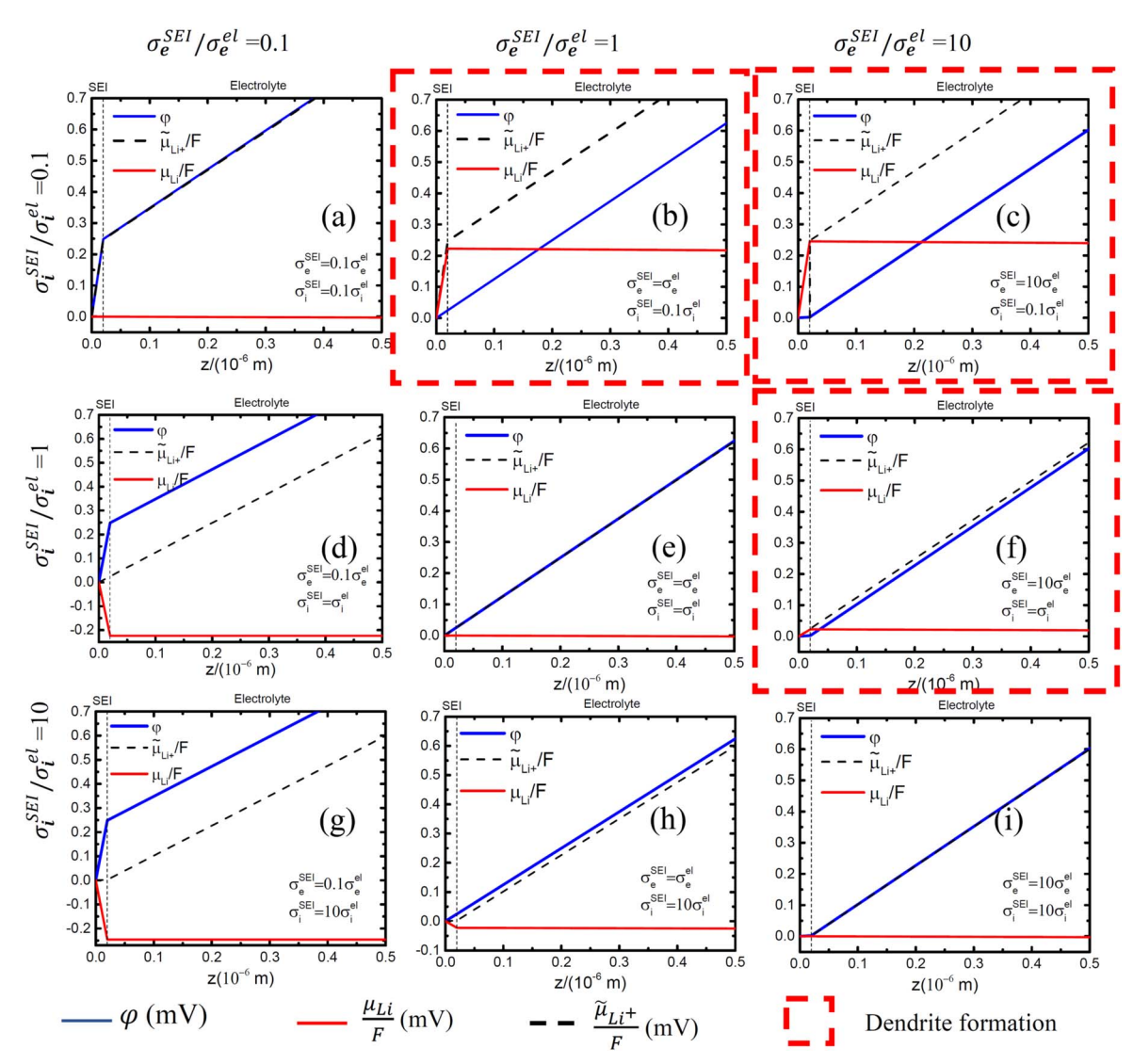


Figure 3. $\frac{\beta_{Li}}{F}$, $\frac{\mu_{Li}}{F}$ and φ near the lithium anode by applying 0.05 V voltage with various electronic and ionic conductivities of SEI layers. The SEI locates from $z_a=0$ to $z_0=2\times 10^{-8}$ m and the other region($z>z_0$) is electrolyte. $\frac{\mu_{Li}}{F}\geq 0$ indicates the possible formation of lithium metal in the electrolyte and the situation is marked with red boxes. If the electrolyte is liquid, the maximum chemical potential is limited to that of pure lithium. In such cases, lithium will precipitate in the electrolyte.

of lithium ions and electrons in the SEI layer. The concentration of electrons is typically low in an electronic insulator, thus the SEI layer with a low σ_e^{SEI} also suppresses lithium precipitation kinetically. Some electronic conductive species in the solid electrolyte are revealed to be responsible for dendrite formation. Also, a low σ_e^{SEI} suppresses the internal leakage which lowers shelf life. Figure 3 also shows the variation of the chemical potential in the electrolyte. If the electrolyte is liquid, the maximum chemical potential corresponds that for pure lithium. If it exceeds this, lithium will precipitate in the electrolyte. If the electrolyte is a solid electrolyte, the precipitated lithium will be under a pressure (b, c and f). Also the equations developed here, in concept, can also be applied to a lithium-ion cell. In such a case, the applied voltage during charging must be greater than the open circuit potential.

As for ionic conductivity, high σ_i^{SEI} is preferred to reduce the energy loss inside the battery during the charging and discharging process. Thus, it is possible to achieve high current density (faster charging rates and high power) and high durability (prevents dendrite formation) simultaneously by achieving an SEI layer with low r_i^a and high r_e^a .

The Growth of a Lithium Precipitate on the SEI/Electrolyte Interface

As shown in Fig. 3, $\frac{\mu_{Li}}{F}$ would reach a maximum value at the boundary between the SEI layer and the electrolyte for the dendrite formation cases ((b), (c) and (f) in Fig. 3). The most likely location for the neutral lithium formation is where the $\frac{\mu_{Li}}{F}$ is the highest. It is interesting to investigate the growth behavior of lithium precipitate (Ω) at the SEI layer and the electrolyte interface. It is important to mention that the magnitudes of the fluxes, however, are time-dependent. The μ_{Li} of the lithium precipitate is the same as lithium metal (for liquid electrolyte), μ_{Li}^a . At the lithium precipitate surface ($\partial\Omega$)

$$\mu_{Li}|_{\partial\Omega} = \mu_{Li}^a \tag{66}$$

The conductivity of lithium metal is about 10^7 S m⁻¹ which allows the precipitate to be treated as an equipotential body.

$$\varphi|_{\partial\Omega} = Constant$$
 [67]

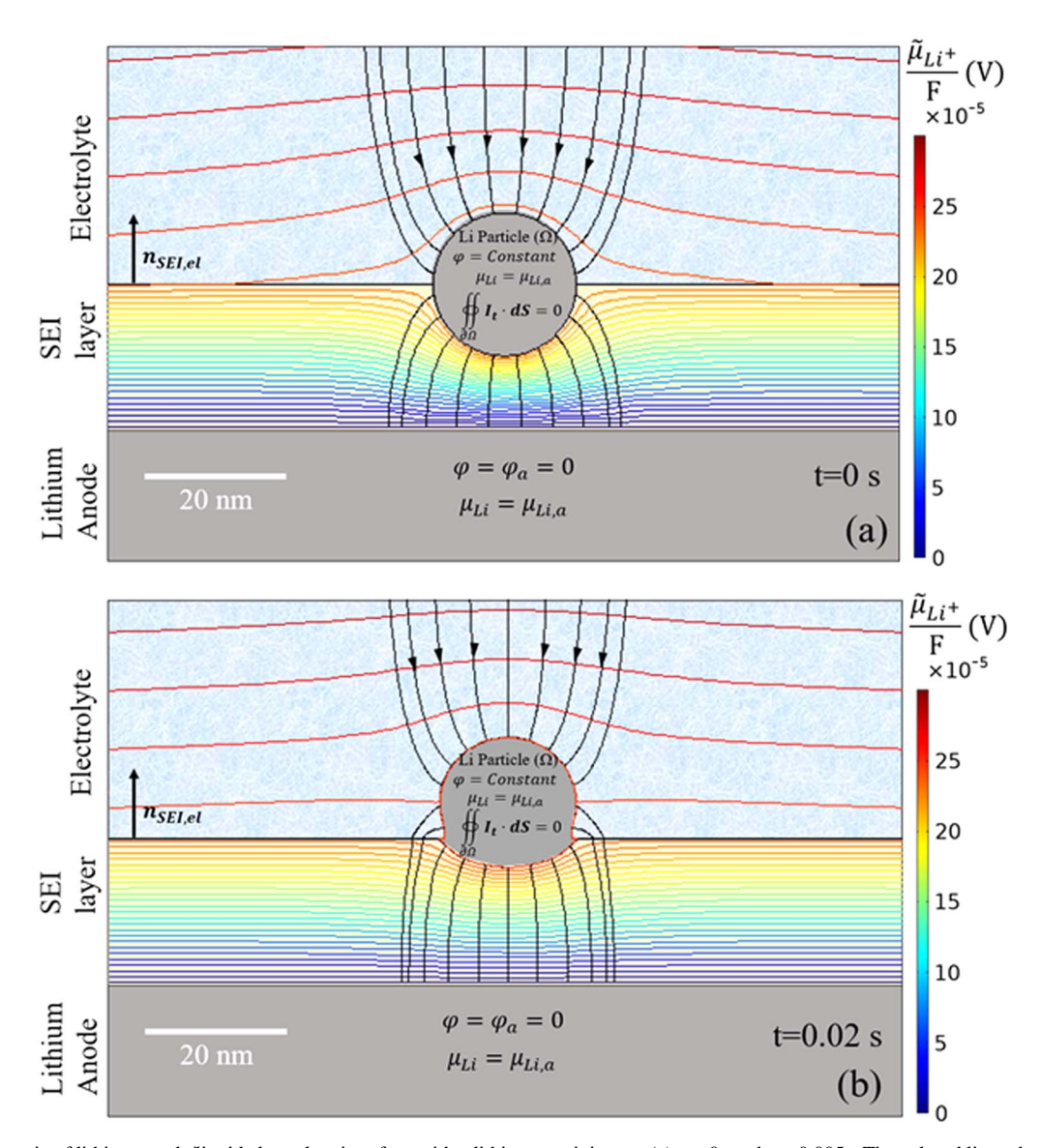


Figure 4. A schematic of lithium anode/liquid electrolyte interface with a lithium precipitate at (a) t=0s and t=0.005s. The colored lines show the contour plot of $\frac{\hat{\mu}_{Li^+}}{F}$ and the black lines with the arrows are the lithium ion fluxes, J_{Li^+} . $\sigma_i^{SEI}=0.1\sigma_i^{el}$ and $\sigma_e^{SEI}=\sigma_e^{el}$.

Besides, the conservation of charge requires that the electrical current that flows into the precipitate is equal to the current that flows out. As we only consider the boundary of the lithium precipitate, Eq. 22 can be rewritten in a surface integral form as Eq. 68 with Gauss's theorem.

$$\oint_{\partial\Omega} \mathbf{I}_t \cdot \mathrm{d}\mathbf{S} = 0$$
[68]

This integration covers the whole surface of the lithium precipitate, $\partial\Omega$. The actual procedure involves solving the equations at various intervals of time, such as Δt , $2\Delta t$, $3\Delta t$ Thus, while Eqs. 21, 22, etc. remain valid, the numerical values change with time.

The growth rate (q) of the lithium surface is proportional to the lithium mass flux which is perpendicular to the surface.

$$q = -V_{Li}(J_{Li} + J_{Li^+}) \cdot n_p$$
 [69]

Where V_{Li} is molar volume of lithium metal and n_p is a normal vector to the lithium surface. From Eq. 24, we learn that the lithium metal flux in the electrolyte is almost 0 in both the electrolyte and the SEI layer.

$$\mathbf{J}_{Li} \sim 0 \tag{70}$$

The growth of the lithium precipitate surface is dominated by the ionic flux, J_{Li^+} , which is driven by the gradient of $\tilde{\mu}_{Li^+}$. J_{Li^+} is proportional to I_i as it is stated in Eq. 26. The Eq. 69 can be rewritten as,

$$q = -\frac{V_{Li}}{F} \mathbf{I}_{i} \cdot \mathbf{n}_{p} \tag{71}$$

Equation 71 illustrates the fact that the growth of lithium precipitate is directly related to the I_i on the lithium precipitate surface.

The neutral lithium evolution is simulated based on a spherical lithium precipitate with a radius of 10 nm embedded between the SEI layer and lithium ion electrolyte, shown in Fig. 4. The thickness of the SEI layer is 20 nm and various σ_i^{SEI} and σ_e^{SEI} are employed to investigate the impact of the SEI layer transport properties. Lithium precipitate is also assumed to be fresh so that no new SEI layer covers its surface in the electrolyte, although, in reality, some SEI layer may form. Figure 4 also shows the contour plot of $\frac{\tilde{\mu}_{Li}+1}{r}$ near the

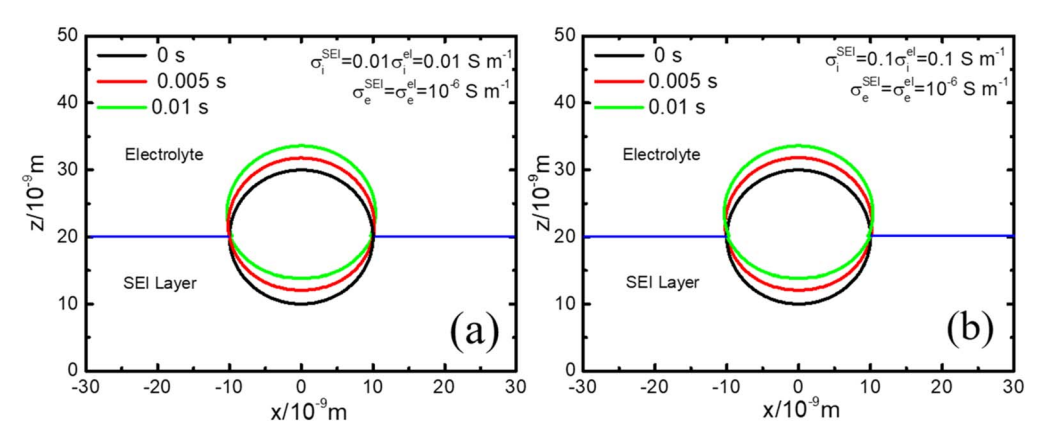


Figure 5. Lithium precipitate growth in a liquid electrolyte at the interface between the electrolyte and SEI layer with different ionic conductivities of the SEI layer (σ_i^{SEI}) . (a) $\sigma_i^{SEI} = 0.1\sigma_i^{el}$ and (b) $\sigma_i^{SEI} = 0.01\sigma_i^{el}$.

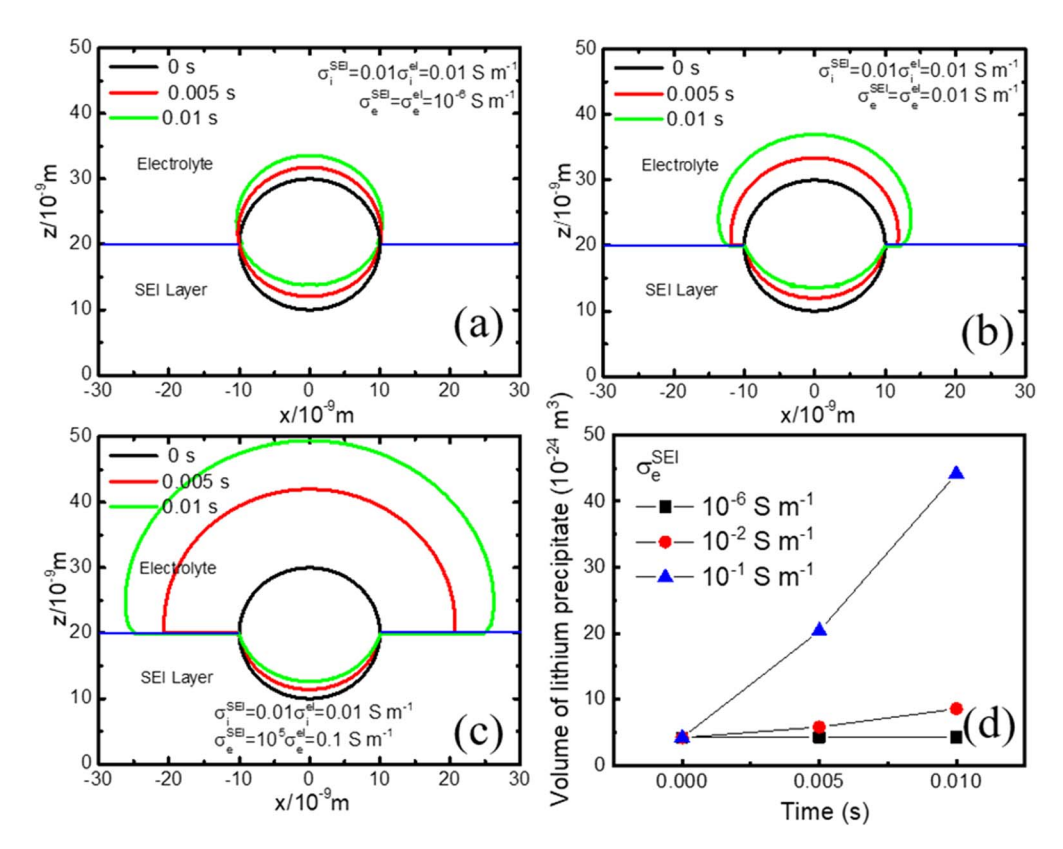


Figure 6. Lithium precipitate growth at electrolyte SEI layer interface in a liquid electrolyte with different electronic conductivities of SEI layer (σ_e^{SEI}). (a) $\sigma_e^{SEI} = \sigma_e^{el}$, (b) $\sigma_e^{SEI} = 10^4 \sigma_e^{el}$, (c) $\sigma_e^{SEI} = 10^5 \sigma_e^{el}$, and (d) the volume of the lithium precipitate changes.

lithium precipitate. The formation of Li precipitate distorts the equipotential lines of $\frac{\tilde{\mu}_{Li^+}}{F}$, which should be parallel with the SEI/electrolyte boundary. The black streamlines with arrows are the lithium ion fluxes which is perpendicular to the equipotential lines of $\frac{\tilde{\mu}_{Li^+}}{F}$ everywhere since the flux is driven by the gradient of $\frac{\tilde{\mu}_{Li^+}}{F}$. The lithium ion flux points toward the top surface of the lithium precipitate and forms the lithium deposit. While the bottom of the lithium precipitate tends to dissolve into the SEI layer and deposit on the lithium electrode.

Figure 5 shows the impact of σ_i^{SEI} values on the growth of the lithium precipitate at the interface. The cross-section of the lithium

precipitate is plotted as a function of time. The top surface is growing into the electrolyte due to the accumulation of the lithium deposit and the bottom surface is dissolving, which agrees with the analysis of the contour plot. Different σ_i^{SEI} does not really change the shape of the lithium precipitate significantly over the range of σ_i^{SEI} selected here for calculations. The spherical precipitate is moving away from the lithium metal anode and loses its connection with the electrodes. It is a typical field driven bipolar plating process which is well studied in Ag⁺ conductive electrolyte that the metal particles in the electrolyte will be polarized and migrate to the positive electrode. ^{31,32} After complete coverage of the less conductive SEI layer on its surface, the particle is isolated and often called "dead lithium" in lithium batteries. The dead lithium forms during the cycling periods embedded in the SEI layer and

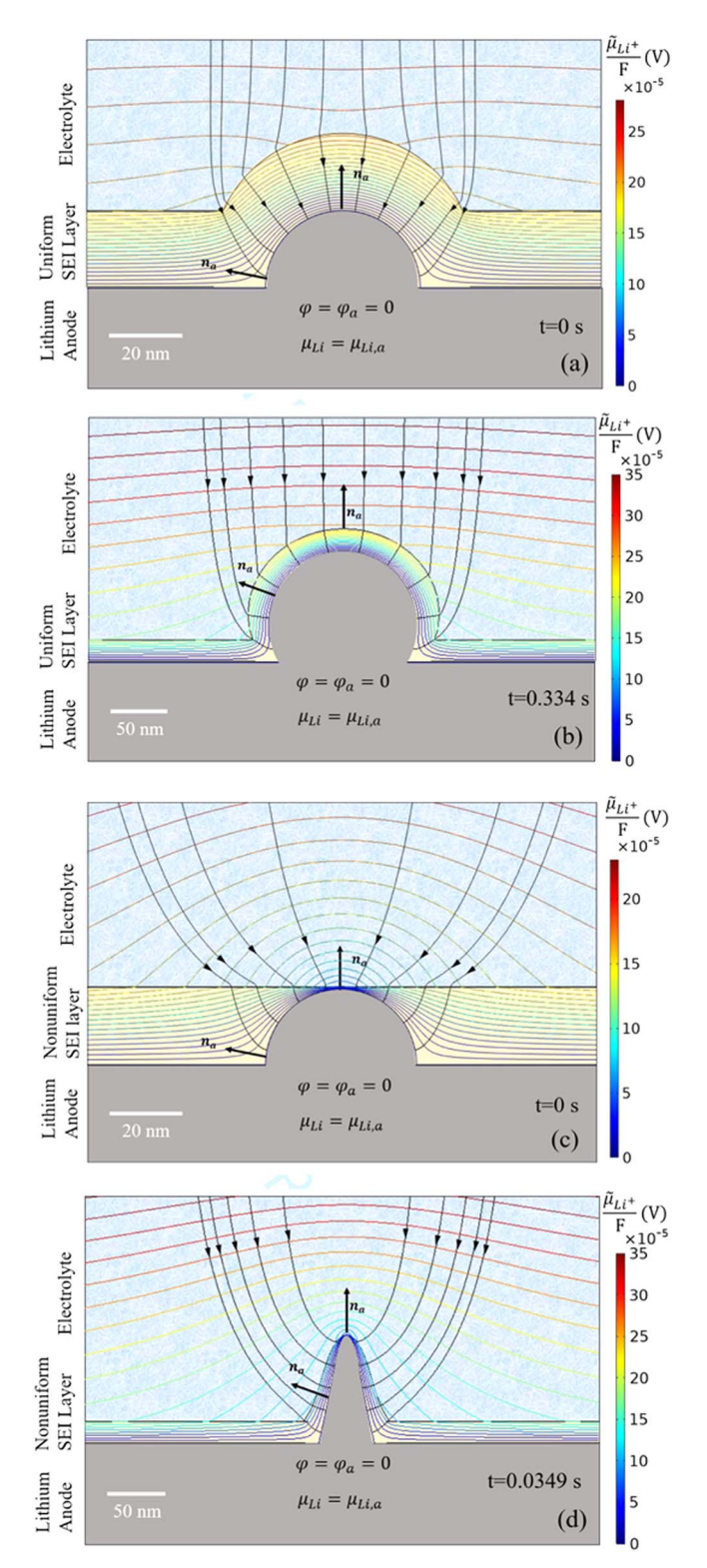


Figure 7. A schematic of dendrite evolution in a liquid electrolyte during lithium electrodeposition on the lithium metal electrode with a uniformly distributed SEI layer at (a) t = 0s (b) t = 0.334s and a nonuniformly distributed SEI layer at (c) t = 0s (d) t = 0.0394s. The colored lines show the contour plots of $\frac{\ddot{\mu}_{Li^+}}{F}$ and the black lines with the arrows are the lithium ion fluxes, J_{Li^+} . $\sigma_i^{SEI, a} = 0.1\sigma_i^{el}$ and $\sigma_e^{SEI, a} = \sigma_e^{el}$.

leads to performance degradation and capacity loss. ^{33,34} The formation and growth of the neutral lithium in the SEI layer can be an origin of the dead lithium formation.

Compared to σ_i^{SEI} , σ_e^{SEI} has a much greater impact on the lithium precipitate growth. By increasing σ_e^{SEI} from 10^{-6} S m⁻¹ up to 10^{-1} S m⁻¹ in Figs. 6a–6c, the top surface of lithium grows significantly. The volume of the precipitate is plotted as a function of time for different σ_e^{SEI} values in Fig. 6d. With a low σ_e^{SEI} , lithium ions carry most of the charge and Eq. 67 leads to conservation of lithium in the precipitate. Theoretically, the volume of lithium should not change if the SEI is a perfect electronic insulator. However, when σ_e^{SEI} increases to 10^{-1} S m⁻¹, electrons become the major charge carrier in the SEI layer. Then lithium starts to precipitate significantly in the electrolyte part with a slight shrinkage of the part in the SEI layer. Any neutral lithium formed outside the anode would lead to capacity loss and reduce the life of a lithium-ion battery. Therefore, the SEI layer has to be designed as a good electronic insulator to prevent or suppress neutral lithium formation and growth in the SEI layer.

The Growth of a Dendrite

The question becomes how a dendrite precursor on the anode will grow into the electrolyte. Figure 7a shows a schematic of lithium dendrite evolution with a uniform SEI layer with the contour plot of $\frac{\bar{\mu}_{Li^+}}{F}$ and streamlines of J_{Li^+} . The growth of the dendrite is modeled with a constant applied potential, 0.05 V. The dendrite precursor is a hemispherical lithium particle with a radius of 19.8 nm which is embedded in the anode SEI layer. We first assume the formation of SEI layer is so fast that the SEI layer on the anode surface and the dendrite surface is uniform with a thickness of 20 nm. The lithium precursor leads to a larger gradient of μ_{Li} near its tip than the bottom part in the electrolyte, indicating lithium prefers to deposit on the tip than at the bottom.

The higher σ_i^{SEI} leads to faster growth into the electrolyte as shown in Fig. 8. Figure 8d shows that the volume of the lithium precipitate increases faster with a higher σ_i^{SEI} . A lower ionic resistance on the lithium surface, increases J_{Li^+} and leads to a faster accumulation of lithium on the precursor. The shape of the precipitate is plotted with the height and time marked accordingly. The deposition of lithium does not only occur on the tip but on all surfaces of the dendrite. The dendrite maintains a spherical or a nearly spherical shape, but its center is moving toward the electrolyte. By increasing the electronic conductivity of the SEI layer by 10,000 times, the growth of lithium precipitate remains exactly the same based on the simulation in Fig. 9. The σ_e^{SEI} value turns out to have no effect on the growth of the lithium precipitate owing to the independency between σ_e^{SEI} and I_i in Eq. 71.

From Eqs. 54 and 56, the I_i depends on the r_i^a values between

anode and electrolyte interface, which is also a function of thickness of SEI layer, δ_a , on the dendrite surface. The lithium precipitate grows into the electrolyte, but the shape of the dendrite is highly dependent on r_i^a distribution on the dendrite surface. In other words, an unevenly distributed ASR and inhomogeneous lithium ion flux on the dendrite surface, owing to the nonuniform thickness of the SEI layer, leads to different shapes of dendrites. In fact, if the SEI formation reaction between lithium metal and the electrolyte solvent is not fast enough, and the limited kinetics can lead to a nonuniform SEI during the lithium deposition. During the lithium dendrite growth, the SEI layer is stretched and becomes thinner locally, which results in an accelerated SEI layer growth. The thickness of the SEI layer at the tip of the dendrite, which is balanced between the SEI growth and the stretch effect of the SEI layer, tends to reach a stable value under a stationary state.³⁵ The thickness of the SEI on the tip at stationary state is assumed to be very thin (0.2 nm) while it on the bottom is equal to the thickness of SEI on the anode surface (20 nm). The distribution of the SEI layer thickness on the dendrite is assumed empirically as following,

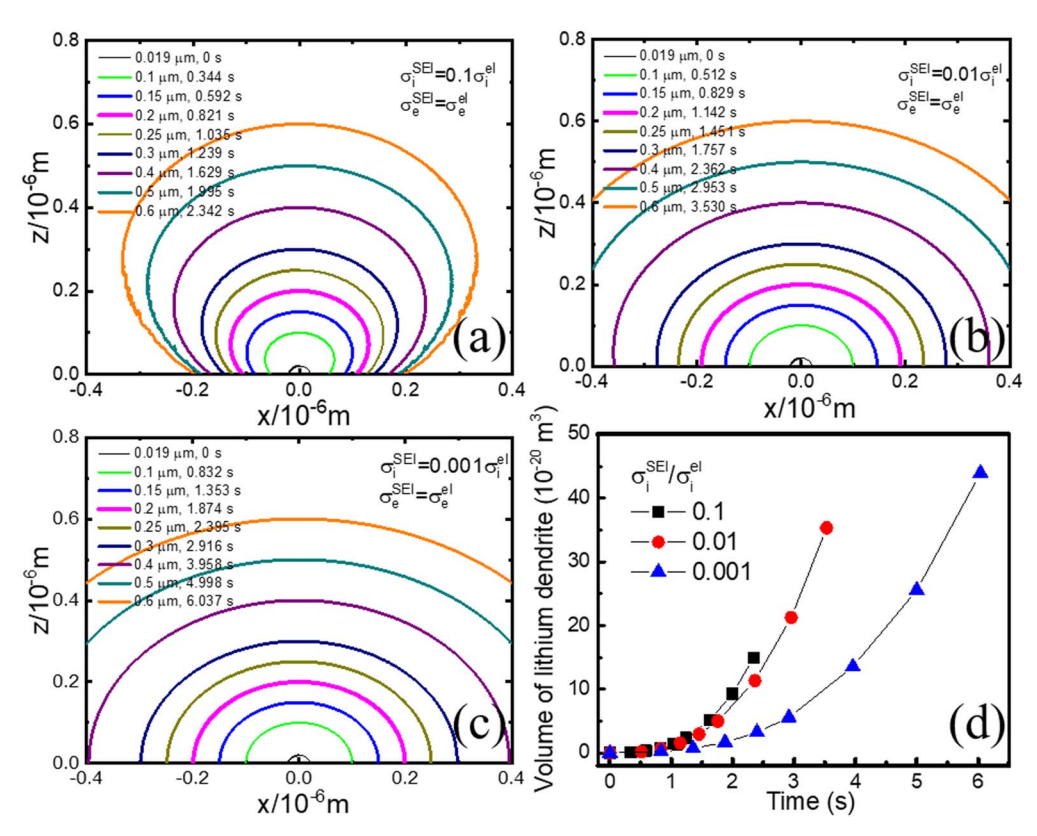


Figure 8. Lithium dendrite growth in a liquid electrolyte with a uniformly distributed SEI layer with different ionic conductivities of SEI layer. (a) $\sigma_i^{SEI} = 0.1 \sigma_i^{el}$, (b) $\sigma_i^{SEI} = 0.01 \sigma_i^{el}$, (c) $\sigma_i^{SEI} = 0.001 \sigma_i^{el}$, and (d) the time dependent volumes of the lithium dendrites.

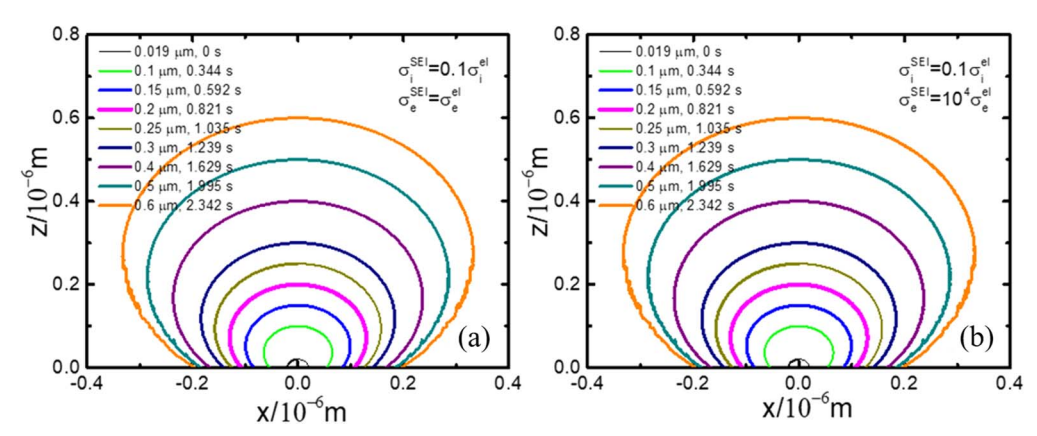


Figure 9. Lithium dendrite growth in a liquid electrolyte with a uniformly distributed SEI layer with different electronic conductivities of the SEI layer. (a) $\sigma_e^{SEI} = \sigma_e^{el}$ and (b) $\sigma_e^{SEI} = 10^4 \sigma_e^{el}$.

$$\delta_a(z) = \left(0.2 + 19.8\sqrt{1 - \left(\frac{z}{z_{tip}}\right)^2}\right) \text{nm}$$
 [72]

Shown in Figs. 7c and 7d are schematics of growth of dendrite with nonuniform SEI layers at different times. The equipotential lines of $\frac{\tilde{\mu}_{Li^+}}{F}$ are highly distorted near the tip of the lithium precursor during the electrochemical deposition. J_{Li^+} has a strong preference to transport through the thinner SEI layer, which is of much lower ionic resistance. Figure 10 shows dendrite growth with different ionic conductivity of the SEI layer. A low conductivity will significantly reduce the growth rate of the surface covered by the

thicker SEI layer. A sharp dendrite shape can be observed when the ion conductivity of the SEI layer is relatively low ($\sigma_i^{SEI}=10^{-1}$, 10^{-2} and 10^{-3} S m⁻¹). While for an assumed high conductivity SEI layer ($\sigma_i^{SEI}=10$ S m⁻¹), the shape of lithium deposit maintains nearly a spherical shape. In contrast to the uniform SEI, the nonuniform SEI layer allows the dendrite covered with the less conductive SEI to grow faster. Though the lower conductivity of the SEI layer tends to reduce the net ionic flux, it also leads to a stronger preference for ionic flux to pass through the thin SEI region on the tip of dendrite. The balance of the two effects allows a maximum lithium accumulation rate when $\sigma_i^{SEI}/\sigma_i^{el}$ is in the range of 0.001 to 0.01 based on Fig. 10e.

In order to quantify the sharpness of the lithium dendrite, the aspect ratio is defined as Eq. 73 in Fig. 11a.

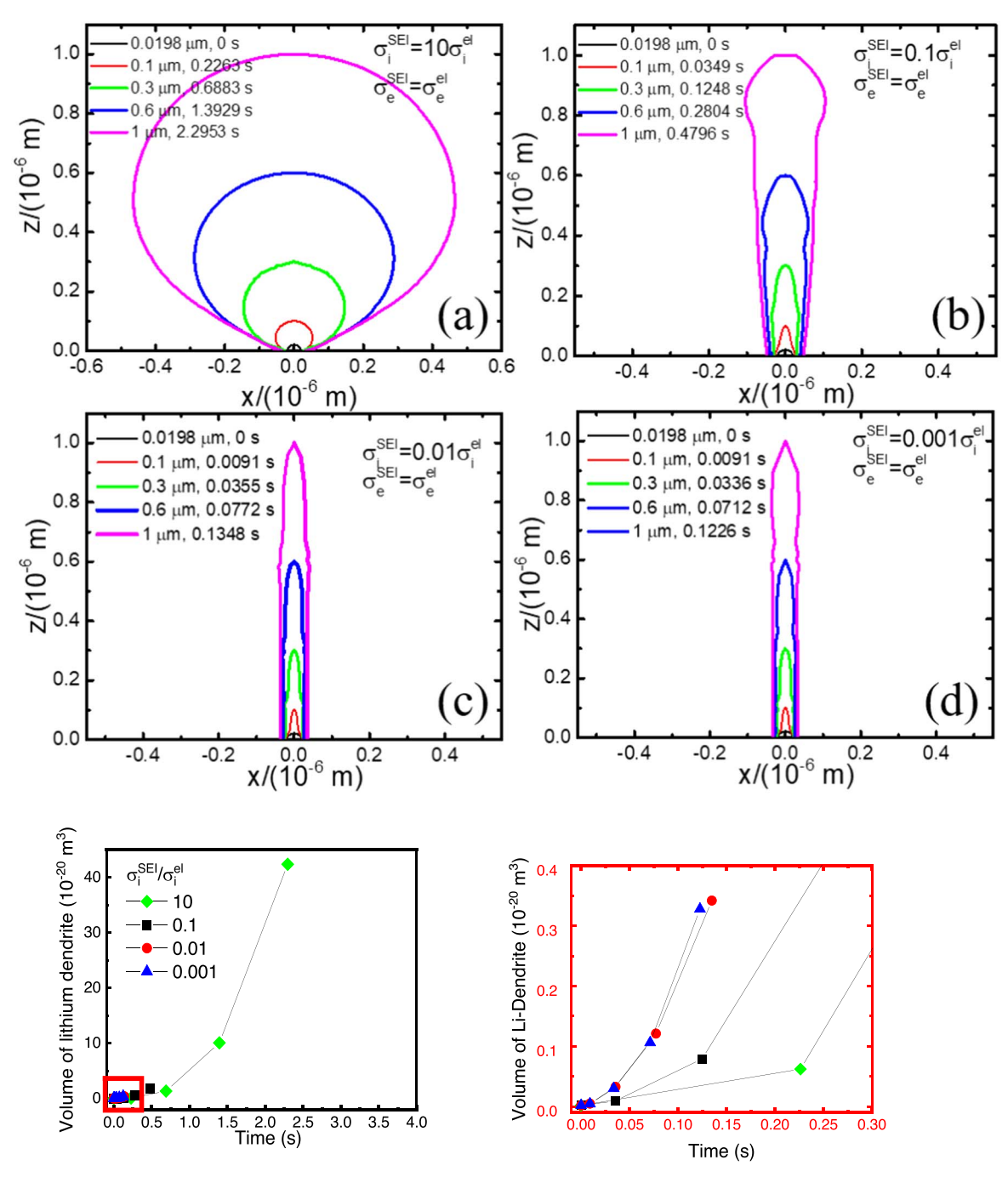


Figure 10. Lithium dendrite growth in a liquid electrolyte with a nonuniformly distributed SEI layer with different ionic conductivities of the SEI layer. (a) $\sigma_i^{SEI} = 10\sigma_i^{el}(b)$ $\sigma_i^{SEI} = 0.1\sigma_i^{el}(c)$ $\sigma_i^{SEI} = 0.01\sigma_i^{el}(d)$ $\sigma_i^{SEI} = 0.001\sigma_i^{el}(d)$ and (e) the time dependent volumes of the lithium dendrites.

Aspect Ratio =
$$\frac{h}{w}$$
 [73]

Where h is the height of the dendrite and w is its diameter at a given dimension along the z direction. The ratio is equal to 1 when the lithium precipitate is a full sphere, it is equal to 0.5 when it is semispherical, and it is equal to 0 when the surface is flat. The higher aspect ratio indicates a sharper dendrite. For a uniform SEI layer in Fig. 11b, the ratio varies from 0.5 to 1 during the dendrite growth for all ionic conductivities. Thus, the dendrite would hardly form when the SEI layer is uniform. On the other hand, the aspect ratio reaches about 4 to 5 when the SEI is nonuniform and with a lower ionic conductivity than that in the electrolyte, shown in Fig. 11c. A thick

insulating SEI layer prevents the dendrite from growing at the bottom part. As the σ_i^{SEI} is lower than 1/100 of σ_i^{el} , the aspect ratio remains almost the same during the dendrite growth. This threshold value will vary with the distribution of SEI layer on the dendrite surface. Thus, to avoid the lithium precipitate from growing into a dendrite, one should either enhance the ionic conductivity of the SEI layer, or make the SEI layer of uniform thickness or both.

Conclusions

The concept of chemical potential of a neutral species in the electrolyte and interfacial layers is used to elucidate the origin of dendrite formation in an SEI layer to calculate the kinetics of metallic lithium precipitation. The metal species grows along with

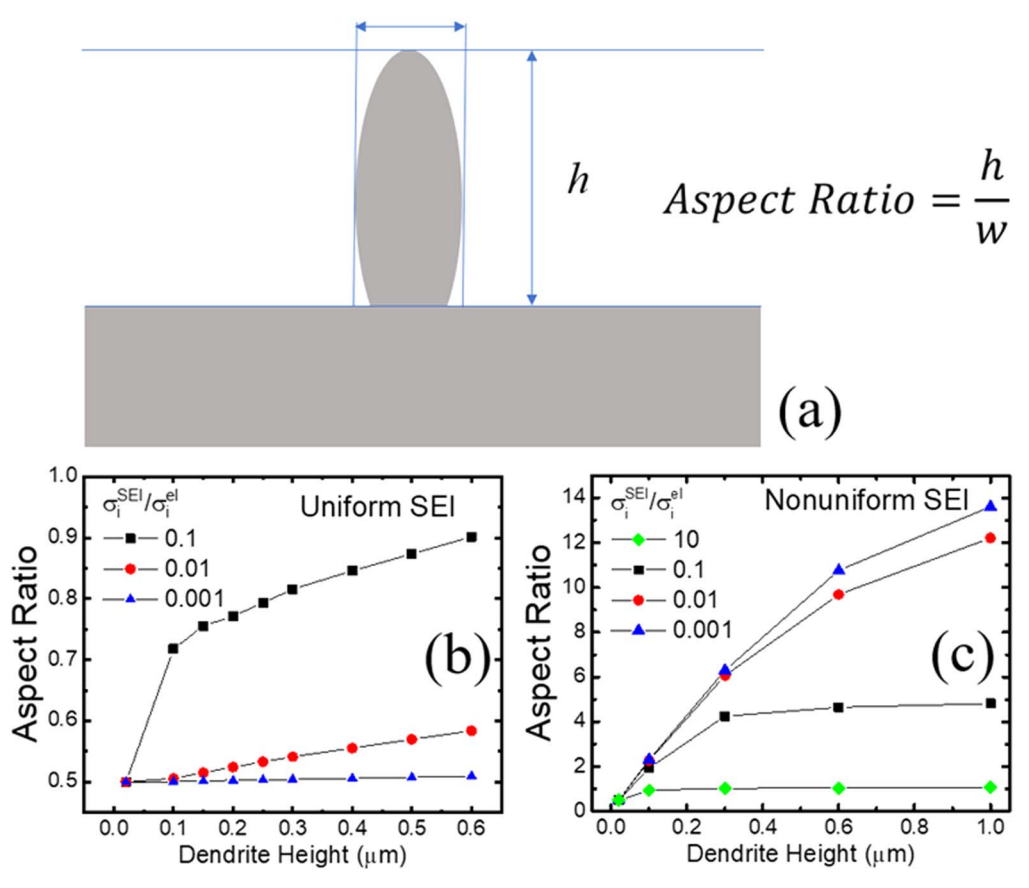


Figure 11. (a) A schematic of the definition of aspect ratio (b) Aspect ratio changes with dendrite height with a uniform SEI layer. (c) Aspect ratio changes with dendrite height with a nonuniform SEI layer.

the electrical current in the electrolyte owing to its much higher conductivity than the electrolyte, works as a part of the electrode, forms the dendrites of different features, and even causes short circuit. Some general conclusions are summarized as follows:

- By applying local thermodynamic and chemical equilibrium and considering the electronic current, two measurable parameters, the chemical potential of a neutral species and the electrical potential, are used to study the deposition kinetics of neutral species at quasi-steady state.
- 2. The high ionic conductivity of the SEI layer reduces the lithium chemical potential in the SEI layer and suppresses lithium precipitate formation. In addition, a higher σ_i^{SEI} allows more homogeneous ion flux on the lithium metal surface and prevents lithium dendrite formation. The high σ_i^{SEI} also leads to faster electrode kinetics, reduced charging time, and less energy loss during cycling. As a result, durability and high performance could be achieved simultaneously through a proper choice of electrolyte/electrode materials that lead to SEI layer with low electronic conductivity and a high ionic conductivity rather than a tradeoff with the optimized properties of the SEI layer.
- 3. The stretching of SEI layer during lithium electrodeposition could lead to nonuniform thickness or even cracks. The nonuniform SEI layer thickness induces a nonuniform ionic current on the lithium electrode surface, which leads to a high aspect ratio over 10 and sharper dendrite geometry. Enhancing mechanical strength and the SEI formation kinetics can improve the stability of the lithium metal electrode. Much has been accomplished to improve the cycling stability of lithium electrode, however, the electronic conductivity of SEI is usually neglected.
- Though the electronic current does not affect the ionic flux on the metal electrode surface, a highly electrically insulating SEI

layer suppresses the formation and growth of lithium precipitate in the SEI layer during charging. Further reducing electronic conduction in the SEI layer would be a more efficient approach than developing an artificial SEI layer with higher ionic conductivity to achieve better durability.

Acknowledgments

This work is supported by the US National Science Foundation under Grant Number OIA-1946231 and the Louisiana Board of Regents for the Louisiana Materials Design Alliance (LAMDA), National Science Foundation under grant number NSF-DMR-1742696, and National Science Foundation under grant number NSF-CBET-1604008.

ORCID

Yudong Wang https://orcid.org/0000-0002-3496-5076 Xiao-Dong Zhou https://orcid.org/0000-0001-9934-9429

References

- X. Sun, M. Chen, Y.-L. Liu, P. Hjalmarsson, S. D. Ebbesen, S. H. Jensen, M. B. Mogensen, and P. V. Hendriksen, J. Electrochem. Soc., 160, F1074 (2013).
- R. Knibbe, M. L. Traulsen, A. Hauch, S. D. Ebbesen, and M. Mogensen, J. Electrochem. Soc., 157, B1209 (2010).
- M. A. Laguna-Bercero, R. Campana, A. Larrea, J. A. Kilner, and V. M. Orera, J. Power Sources, 196, 8942 (2011).
- K. N. Wood, E. Kazyak, A. F. Chadwick, K.-H. Chen, J.-G. Zhang, K. Thornton, and N. P. Dasgupta, ACS Central Science, 2, 790 (2016).
- D. Aurbach, E. Zinigrad, Y. Cohen, and H. Teller, Solid State Ionics, 148, 405 (2002).
- F. Han, A. S. Westover, J. Yue, X. Fan, F. Wang, M. Chi, D. N. Leonard, N. J. Dudney, H. Wang, and C. Wang, *Nat. Energy*, 4, 187 (2019).
- X. Gao, Y.-N. Zhou, D. Han, J. Zhou, D. Zhou, W. Tang, and J. B. Goodenough, *Joule*, 4, 1864 (2020).

- 8. A. V. Virkar, J. Power Sources, 147, 8 (2005).
- 9. A. V. Virkar, J. Power Sources, 196, 5970 (2011).
- 10. D. Kondepudi and I. Prigogine, Modern Thermodynamics: from Heat Engines to Dissipative Structures (Wiley, Singapore) (2015).

 11. L. Zhang, L. Zhu, and A. V. Virkar, J. Electrochem. Soc., 166, F1275 (2019).
- 12. Y. Dong and I. W. Chen, Acta Mater., 156, 399 (2018).
- 13. A. V. Virkar, Int. J. Hydrogen Energy, 35, 9527 (2010).
- 14. H.-H. Sun, A. Dolocan, J. A. Weeks, R. Rodriguez, A. Heller, and C. B. Mullins, J. Mater. Chem. A, 7, 17782 (2019).
- 15. Z. Huang, J. Ren, W. Zhang, M. Xie, Y. Li, D. Sun, Y. Shen, and Y. Huang, Adv. Mater., 30, 1803270 (2018).
- 16. C. Monroe and J. Newman, J. Electrochem. Soc., 151, A880 (2004).
- 17. K. Xu, Chem. Rev., 104, 4303 (2004).
- 18. M. Aydinol, A. Kohan, and G. Ceder, J. Power Sources, 68, 664 (1997).
- 19. S. Gao, F. Sun, N. Liu, H. Yang, and P.-F. Cao, Mater. Today, 40, 140 (2020).
- 20. X.-B. Cheng, C. Yan, H.-J. Peng, J.-Q. Huang, S.-T. Yang, and Q. Zhang, Energy Storage Mater., 10, 199 (2018).
- 21. B. Boukamp and R. Huggins, Mater. Res. Bull., 13, 23 (1978).
- 22. Y. Liu, D. Lin, P. Y. Yuen, K. Liu, J. Xie, R. H. Dauskardt, and Y. Cui, Adv. Mater., 29, 1605531 (2017).

- 23. J.-Z. Kong, C. Ren, Y.-X. Jiang, F. Zhou, C. Yu, W.-P. Tang, H. Li, S.-Y. Ye, and J.-X. Li, J. Solid State Electrochem., 20, 1435 (2016).
- 24. J.-I. Lee, M. Shin, D. Hong, and S. Park, *Adv. Energy Mater.*, **9**, 1803722 (2019).
- 25. M. S. Grewal, M. Tanaka, and H. Kawakami, Electrochim. Acta, 307, 148 (2019).
- 26. K. Liu, A. Pei, H. R. Lee, B. Kong, N. Liu, D. Lin, Y. Liu, C. Liu, P.-C. Hsu, and Z. Bao, JACS, 139, 4815 (2017).
- C. Li, L. Gu, and J. Maier, *Adv. Funct. Mater.*, 22, 1145 (2012).
 Y. Zhong, Y. Chen, Y. Cheng, Q. Fan, H. Zhao, H. Shao, Y. Lai, Z. Shi, X. Ke, and Z. Guo, ACS Appl. Mater. Interfaces, 11, 37726 (2019).
- 29. K. Deng, D. Han, S. Ren, S. Wang, M. Xiao, and Y. Meng, J. Mater. Chem. A, 7, 13113 (2019).
- 30. C. Yang, B. Liu, F. Jiang, Y. Zhang, H. Xie, E. Hitz, and L. Hu, Nano Res., 10, 4256 (2017).
- 31. K. Peppler, C. Reitz, and J. Janek, Appl. Phys. Lett., 93, 074104 (2008).
- 32. Y. Yang, P. Gao, L. Li, X. Pan, S. Tappertzhofen, S. Choi, R. Waser, I. Valov, and W. D. Lu, Nat. Commun., 5, 4232 (2014).
- 33. K.-H. Chen, K. N. Wood, E. Kazyak, W. S. LePage, A. L. Davis, A. J. Sanchez, and N. P. Dasgupta, J. Mater. Chem. A, 5, 11671 (2017).
- 34. A. Sarkar, I. C. Nlebedim, and P. Shrotriya, J. Power Sources, 502, 229145 (2021).
- 35. G. Liu and W. Lu, J. Electrochem. Soc., 164, A1826 (2017).